Open Access Library Journal
2026, Volume 13, e16127
ISSN Online: 2333-9721
ISSN Print: 2333-9705

Spatiotemporal Patterns Induced by Nonlocal Spatial Memory and Nonlocal Interaction

Jiajia Tang, Yanfei Du*

School of Mathematics and Data Science, Shaanxi University of Science and Technology, Xi'an, China
Email: *duyanfei@sust.edu.cn

How to cite this paper: Tang, J.J. and Du, Y.F. (2026) Spatiotemporal Patterns Induced by Nonlocal Spatial Memory and Nonlocal Interaction. *Open Access Library Journal*, **13**: e16127.
https://doi.org/10.4236/oalib.1116127

Received: October 5, 2026
Accepted: November 13, 2026
Published: November 16, 2026

Copyright © 2026 by author(s) and Open Access Library Inc.
This work is licensed under the Creative Commons Attribution International License (CC BY 4.0).
http://creativecommons.org/licenses/by/4.0/
Open Access

Abstract

In this paper, we formulate a reaction-diffusion model incorporating nonlocal spatial memory and nonlocal interaction, where the spatial memory kernel is characterized by the Green function, which describes that memory decays with spatial distance. In the absence of memory delay, linear stability analysis reveals that the system can undergo Turing bifurcation, which may induce spatially nonhomogeneous steady states. When the strength of local interaction $a \geq 0$, the linear instability only occurs for the 1-mode; while for $a < 0$, linear instability can arise for arbitrary modes, and Turing-Turing bifurcation may take place. When memory delay is incorporated, we derive the stability regions of the equilibrium u_* for any τ on the plane spanned by the diffusion coefficient and the memory-based diffusion coefficient. We also obtain partial stability regions of u_*: within such regions, u_* is asymptotically stable for $\tau < \tau_*$, and linear instability emerges for $\tau > \tau_*$, which may give rise to spatially inhomogeneous periodic solutions. For fixed d_1, on the plane of the memory-based diffusion coefficient and memory delay, we derive Hopf bifurcation curves for different modes, and Hopf-Hopf bifurcation may occur at the intersections of these curves.

Subject Areas

Dynamical System

Keywords

Nonlocal Spatial Memory, Nonlocal Interaction, Bifurcation, Spatiotemporal Patterns

1. Introduction

Spatial memory and cognitive ability are crucial factors governing the movement

behaviors of animals [1]. To characterize the memory-driven movement of animal populations, Shi *et al.* [2] established a single-species spatial memory model expressed as follows:

$$u_t = d_1 u_{xx} + d_2 \left(u \left(u_\tau \right)_x \right)_x + f(u). \tag{1}$$

This model assumes localized spatial memory and interaction among individuals. Subsequent studies have further incorporated nonlocal memory and nonlocal interaction effects to improve the ecological rationality of the model. Song *et al.* [3] introduced a spatial average kernel integral term into the reaction function to describe nonlocal effects, and verified that only mode-1 stable spatial patterns can form in such systems. An *et al.* [4] considered a single-species reaction-diffusion model with memory delay, nonlocal maturation delay and hostile Dirichlet boundary conditions. The study reveals that memory-based diffusion can induce novel spatiotemporal patterns. Moreover, the pattern structures of periodic solutions under Dirichlet boundary conditions are different from the checkerboard-type patterns in the Neumann-boundary case; striped patterns arise under Dirichlet boundary conditions.

Shi *et al.* [5] (2021) considered that animals' spatial memory does not merely rely on information from a single moment in the past, and memory undergoes biological processes of formation and temporal decay, it is more realistic to characterize the generation and decay of memory by means of distributed delays. A single-species reaction-diffusion model with spatiotemporally distributed memory-based diffusion is established. The time kernels of Gamma-distribution are adopted to distinguish the weak memory kernel from the strong memory kernel, and the Green's function of the diffusion equation is utilized to realize spatially non-local memory. It is obtained that only spatial steady-state patterns can be generated under the weak-kernel case. For the strong-kernel case, spatially inhomogeneous steady states as well as spatially inhomogeneous time-periodic patterns can emerge. The mean time delay of memory can alter the spatial modes of patterns, and pattern formation requires the intensity of memory-based diffusion to exceed a critical threshold. Shi and Song [6] noted that in reality, animals' memory does not only store local information at their own current position x from a single past moment $t-\tau$. As animals move, they can acquire population-distribution information of the entire habitat from past time. Their memory covers the whole spatial domain rather than being restricted to their own location. Accordingly, memory is generalized to spatially global non-local memory, and a single-species reaction-diffusion model is constructed. The results show that time delay exerts no influence under weakly memory-driven movement. For strongly memory-driven movement, a small memory delay destabilizes the homogeneous steady state, whereas a sufficiently large memory delay enhances the stability of the homogeneous equilibrium. Delay-induced Hopf bifurcations can generate spatially inhomogeneous periodic patterns, and multiple stability switches may even occur.

To achieve a more realistic description of nonlocal spatial memory, Xue *et al.* [7] modified the derivative term $(u_\tau)_x$ by substituting it with an integral term equipped with a top-hat kernel function. The corresponding kernel is defined as $K(x,y)=1/(2R)$ for $|x-y|\le R$ and $K(x,y)=0$ otherwise. Ecologically, animal memory intensity decays monotonically with the spatial distance $|x-y|$, namely, animals retain stronger memory of nearby habitats than distant regions. In this context, the Green function [8] [9] serves as a more appropriate kernel function to reflect the distance-dependent attenuation characteristics of animal spatial memory.

Based on the above research, this paper investigates the combined effects of nonlocal memory and nonlocal interaction with the model provided by

$$\begin{cases} \dfrac{\partial u}{\partial t}=d_1\dfrac{\partial^2 u}{\partial x^2}+d_2\dfrac{\partial}{\partial x}\left(u\dfrac{\partial v_\tau}{\partial x}\right)+f(u,G\circ u), & x\in(0,l\pi),t>0,\\ u_x(0,t)=u_x(l\pi,t)=0, & t>0,\\ u(x,t)=\varphi(x,t), & x\in(0,l\pi),t\in[-\tau,0], \end{cases} \tag{2}$$

where $u=u(x,t)$ is the population density of species u at space x and time t, d_1 is the random diffusion coefficient, d_2 is the memory-based diffusion coefficient, Positive values of the memory-based diffusion coefficient ($d_2>0$) represent avoidance of higher remembered population density, while negative values ($d_2<0$) represent attraction toward regions with high remembered population density. and

$$v_\tau(x,t)=K\circ u_\tau(x,t)=\int_0^{l\pi}K(x,y)u(y,t-\tau)\mathrm{d}y, G\circ u=\int_0^{l\pi}G(x,y)u(y,t)\mathrm{d}y,$$

where $K(x,y)$ is the Green function of the operator $-d_1\dfrac{\partial^2}{\partial x^2}+I$ with Neumann boundary condition. *i.e.*, the solution of

$$\begin{cases} -d_1\dfrac{\partial^2 K}{\partial x^2}+K=\delta(x-y), & x\in(0,l\pi),\\ K_x(0,y)=K_x(l\pi,y)=0. \end{cases} \tag{3}$$

τ denotes the memory delay, which indicates that animal movement depends on the population-density gradient at τ time-units in the past. The Green's function $K(x,y)$ describes animals' perception of resources, where nearby resources are perceived more strongly than distant ones. Chen [9] and Ni *et al.* [8] provide more comprehensive biological interpretations for the Green's function. $G(x,y)$ is a valid integral kernel, and we take $G(x,y)=1/(l\pi)$ in this paper. In this model, the spatial scale of the memory kernel $K(x,y)$ is determined by the random diffusion coefficient d_1. Biologically, this choice assumes that the spatial range over which individuals perceive remembered population information is consistent with the characteristic spatial scale of their random movement. Mathematically, $K(x,y)$ is the Green function of the operator $-d_1\partial_{xx}+I$, so variations in d_1 simultaneously modulate two ecological processes: it adjusts the magnitude of random dispersal motion, and also controls the spatial decay rate of

the memory kernel, which governs the spatial smoothing of remembered population information.

The present work extends the studies in [5]-[7], which investigated spatial movement driven solely by nonlocal spatial memory without incorporating nonlocal interaction. In contrast to these references, we couple the Green-function-based memory kernel with an additional nonlocal interaction term. This coupling enables new findings on stability and mode selection: the strength of local interaction a governs the admissible unstable modes. When $a \geq 0$, only mode-1 instability can occur, whereas arbitrary modes may lose stability for $a < 0$, giving rise to Turing-Turing bifurcation. Furthermore, we analyze delay-induced instabilities and derive Hopf bifurcation curves as well as Hopf-Hopf bifurcation points, yielding parameter-dependent stability regions that are not reported in [5]-[7].

The remainder of this paper is organized as follows. Section 2 discusses the stability of homogeneous steady states, derives the critical conditions for Turing bifurcations and delay-induced bifurcations, and partition the parameter regions corresponding to different dynamical behaviours. Section 3 provides an example for numerical simulation to verify the theoretical results, and explores the joint effects of memory delay and non-local interactions on the formation of population spatial patterns.

2. Stability and Bifurcations Analysis

Let $u = u_* > 0$ denote the homogeneous steady state of (2). The linearized system of (2) at u_* is

$$\frac{\partial u(x,t)}{\partial t} = d_1 u_{xx} + d_2 u_* v_{xx}(x,t-\tau) + au + b(G \circ u), \tag{4}$$

where

$$a = \left.\frac{\partial f(u, G\circ u)}{\partial u}\right|_{(u_*,u_*)}, \quad b = \left.\frac{\partial f(u, G\circ u)}{\partial (G\circ u)}\right|_{(u_*,u_*)}.$$

Let $u(x,t) = u_0 \cos\frac{n}{l}x e^{\lambda_n t}$ be the solution to the Equation (4). Using integration by part and the boundary conditions in (3), we have

$$\int_0^{l\pi} K(x,y)\cos\left(\frac{ny}{l}\right)\mathrm{d}y = -\frac{1}{\frac{n^2}{l^2}}\int_0^{l\pi} K_{yy}(x,y)\cos\left(\frac{ny}{l}\right)\mathrm{d}y.$$

From (3) and the symmetry of the Green function, the above equation equals to

$$\begin{aligned}&-\frac{1}{d_1\frac{n^2}{l^2}}\int_0^{l\pi}\left(K(x,y)-\delta(y-x)\right)\cos\left(\frac{ny}{l}\right)\mathrm{d}y\\ &=-\frac{1}{d_1\frac{n^2}{l^2}}\int_0^{l\pi} K(x,y)\cos\left(\frac{ny}{l}\right)\mathrm{d}y+\frac{1}{d_1\frac{n^2}{l^2}}\cos\left(\frac{nx}{l}\right),\end{aligned}$$

which implies that

$$\int_0^{l\pi} K(x,y)\cos\left(\frac{ny}{l}\right)\mathrm{d}y = \frac{1}{1+d_1\frac{n^2}{l^2}}\cos\left(\frac{nx}{l}\right).$$

The characteristic equation of (4) is given by

$$\begin{cases} \lambda_0 = a+b, & n=0, \\ \lambda_n = -d_1\frac{n^2}{l^2} - \frac{d_2 u_* \frac{n^2}{l^2}\mathrm{e}^{-\lambda\tau}}{1+d_1\frac{n^2}{l^2}} + a, & n\in\mathbb{N}. \end{cases} \tag{5}$$

Throughout the rest of this paper, we assume that $a+b<0$, which guarantees that u_* serves as an asymptotically stable equilibrium of the ODE system $u' = f(u,u)$.

2.1. Turing Bifurcation

We first consider the case without memory delay. When $\tau = 0$, the characteristic Equation (5) becomes

$$\lambda_n = -d_1\frac{n^2}{l^2} - \frac{d_2 u_* \frac{n^2}{l^2}}{1+d_1\frac{n^2}{l^2}} + a, n\in\mathbb{N}. \tag{6}$$

Furthermore, we can obtain $\lambda_n > 0$ for $d_2 < d_{2,n}^T(d_1)$, where

$$d_{2,n}^T(d_1) \triangleq -\frac{d_1}{u_*} + \frac{1}{u_*}\left(a\frac{l^2}{n^2} + ad_1 - d_1^2\frac{n^2}{l^2}\right). \tag{7}$$

Now we investigate some properties for the curve $d_2 = d_{2,n}^T(d_1)$.

Proposition 1. *Assume that* $a+b<0$.

1) When $a\geq 0$, $d_2 = d_{2,n}^T(d_1)$ is decreasing with the increasing of n for fixed d_1.

2) Assume that $a<0$.

(i) The curve $d_2 = d_{2,n}^T(d_1)$ is decreasing with the increasing of d_1;

(ii) $d_{2,n}^T(0)$ is increasing with n and $\lim_{n\to+\infty} d_{2,n}^T(0) = 0$;

(iii) The curves $d_2 = d_{2,n}^T(d_1)$ and $d_2 = d_{2,n+1}^T(d_1)$ intersect at $d_1 = d_{1g}^{(n)} = \frac{l^2}{n(n+1)}\sqrt{-a}$, which is decreasing with n, and $d_{2,n}^T\left(d_{1g}^{(n)}\right) = \frac{l^2}{u_*}\left(\frac{a}{n^2} + \frac{a-1}{n(n+1)}\sqrt{-a} + \frac{a}{(n+1)^2}\right)$, which is increasing with n.

Proof. When $a\geq 0$ and $a+b<0$, differentiating both sides of Equation (7) with respect to n, we can obtain

$$\frac{\mathrm{d}d_{2,n}^T(d_1)}{\mathrm{d}n} = -\frac{1}{u_*}\left(\frac{2al^2}{n^3} + \frac{2nd_1^2}{l^2}\right) < 0, \tag{8}$$

and then $d_{2,n}^{T}(d_1)$ is decreasing with n. The conclusion (i) is proved.

When $a<0$, $\frac{1}{u_*}\left(a\frac{l^2}{n^2}+ad_1-d_1^2\frac{n^2}{l^2}\right)<0$. Therefore, $d_{2,n}^{T}(d_1)<0$ for $n\in\mathbb{N}$. By (7), we have

$$\frac{\mathrm{d}d_{2,n}^{T}(d_1)}{\mathrm{d}d_1}=-\frac{1}{u_*}+\frac{1}{u_*}\left(a-2\frac{n^2}{l^2}d_1\right)<0. \tag{9}$$

This implies that the curve $d_2=d_{2,n}^{T}(d_1)$ is decreasing for $d_1>0$. In addition, notice that when $d_1=0$

$$d_{2,n}^{T}(0)=\frac{al^2}{u_*n^2}<0,$$

which is increasing with n and $\lim_{n\to+\infty}d_{2,n}^{T}(0)=0$.

Solving $d_{2,n}^{T}(d_1)=d_{2,n+1}^{T}(d_1)$ for d_1, we have

$$d_1=d_{1g}^{(n)}=\frac{l^2}{n(n+1)}\sqrt{-a}. \tag{9}$$

It is obvious that $d_{1g}^{(n)}$ is decreasing with n. Substituting $d_1=d_{1g}^{(n)}$ into (7), we have

$$d_{2,n}^{T}\left(d_{1g}^{(n)}\right)=\frac{l^2}{u_*}\left(\frac{a}{n^2}+\frac{a-1}{n(n+1)}\sqrt{-a}+\frac{a}{(n+1)^2}\right).$$

Furthermore, we can obtain

$$\frac{\mathrm{d}d_{2,n}^{T}\left(d_{1g}^{(n)}\right)}{\mathrm{d}n}=\frac{l^2}{u_*}\left(\frac{-2a}{n^3}+\frac{(1-a)(2n+1)}{(n^2+n)^2}\sqrt{-a}+\frac{-2a}{(n+1)^3}\right)>0, \tag{10}$$

which tells us that $d_{2,n}^{T}\left(d_{1g}^{(n)}\right)$ is increasing with n. The conclusion (ii) is proved.

From proposition 1(ii), when $a<0$, we define

$$d_{2,T}^{*}(d_1)=\begin{cases}d_{2,1}^{T}(d_1), & d_1>d_{1g}^{(1)},\\ d_{2,j}^{T}(d_1), & d_{1g}^{(j)}\le d_1\le d_{1g}^{(j-1)},\ j=2,3,\cdots.\end{cases} \tag{11}$$

Then we can prove the following results on the stability and bifurcation for u_*.

Lemma 1. Assume that $a+b<0$, $\tau=0$, $d_{2,T}^{*}(d_1)$ is defined by (11).

i) For $a\ge 0$, when $d_2>d_{2,1}^{T}(d_1)$, $\lambda_n<0$ for any $n\in\mathbb{N}_0$. When $d_2<d_{2,1}^{T}(d_1)$, there exists some $n\in\mathbb{N}$ such that $\lambda_n>0$.

ii) For $a<0$, when $d_2>d_{2,T}^{*}(d_1)$, $\lambda_n<0$ for any $n\in\mathbb{N}_0$. When $d_2<d_{2,T}^{*}(d_1)$, there exists some $n\in\mathbb{N}$ such that $\lambda_n>0$.

Proof. From proposition 1 (i), if $d_2>d_{2,1}^{T}(d_1)$, $d_2>d_{2,n}^{T}(d_1)$ for any $n\ge 1$, and all roots of Equation (6) are negative. In addition, for $d_2<d_{2,1}^{T}(d_1)$, there exists some n such that $\lambda_n>0$. For fixed $n\in\mathbb{N}$, Equation (6) has the root $\lambda_n=0$ provided that $d_2=d_{2,n}^{T}(d_1)$, the conclusion (i) is proved.

From proposition 1 (ii), when $d_2 > d_{2,T}^*(d_1)$, $\lambda_n < 0$ for any $n \in \mathbb{N}$, and exists at least one $\lambda_n > 0$ for $d_2 < d_{2,T}^*(d_1)$, the conclusions (ii) follow immediately.

Taking the derivative of both sides of Equation (6) with respect to d_2, we get

$$\left[\frac{\mathrm{d}\lambda}{\mathrm{d}d_2}\right]_{d_2=d_{2,n}^T} = -\frac{u_* \dfrac{n^2}{l^2}}{1+d_1\dfrac{n^2}{l^2}} < 0,$$

the transversality condition holds.

Theorem 1. Assume that $a+b<0$, $\tau=0$ and $d_{1g}^{(n)}$, $d_{2,T}^*(d_1)$ is defined by (9) and (11).

i) When $a \geq 0$, u_* is asymptotically stable for $d_2 > d_{2,1}^T(d_1)$ and unstable for $d_2 < d_{2,1}^T(d_1)$. Moreover, steady state bifurcations occur at $d_2 = d_{2,n}^T(d_1)$;

ii) When $a<0$, u_* is asymptotically stable for $d_2 > d_{2,T}^*(d_1)$ and unstable for $d_2 < d_{2,T}^*(d_1)$, system (2) undergoes Turing bifurcation at $d_2 = d_{2,T}^*(d_1)$. More specifically, for $d_1 \in \left(d_{1g}^{(n)}, d_{1g}^{(n-1)}\right)$ with $n \in \mathbb{N}$, system (2) undergoes mode-n Turing at $d_2 = d_{2,n}^T(d_1)$. Moreover, system (2) undergoes Turing-Turing bifurcation at $(d_1,d_2) = \left(d_{1g}^{(n)}, d_{2,n}^T\left(d_{1g}^{(n)}\right)\right)$ with $n \in \mathbb{N}$ due to interaction of mode-n Turing and mode-$(n+1)$ Turing.

2.2. Spatially Nonhomogeneous Hopf Bifurcation

In this subsection, we investigate the joint effect of the nonlocal interaction and memory delay on the spatiotemporal patterns. For $\tau > 0$, consider the second equation of (5)

$$\lambda_n = -d_1\frac{n^2}{l^2} - \frac{d_2 u_* \dfrac{n^2}{l^2}\mathrm{e}^{-\lambda_n\tau}}{1+d_1\dfrac{n^2}{l^2}} + a, n \in \mathbb{N}. \tag{12}$$

Letting $\lambda_n = i\omega(\omega>0)$ be the solution of Equation (12) and substituting it into (12), we have

$$\begin{cases} \sin\omega\tau = \dfrac{1+d_1\dfrac{n^2}{l^2}}{d_2 u_*}\cdot\omega\dfrac{l^2}{n^2}, \\ \cos\omega\tau = \dfrac{\left(1+d_1\dfrac{n^2}{l^2}\right)\left(a-d_1\dfrac{n^2}{l^2}\right)}{d_2 u_*}\cdot\dfrac{l^2}{n^2}, \end{cases} \tag{13}$$

which implies that

$$\omega^2 = \left(\frac{d_2 u_*}{1+d_1\dfrac{n^2}{l^2}}\cdot\frac{n^2}{l^2} - a + d_1\frac{n^2}{l^2}\right)\left(\frac{d_2 u_*}{1+d_1\dfrac{n^2}{l^2}}\cdot\frac{n^2}{l^2} + a - d_1\frac{n^2}{l^2}\right). \tag{14}$$

Set

$$d_{2,n}^{H}(d_1) \triangleq \frac{d_1}{u_*} + \frac{1}{u_*}\left(d_1^2 \frac{n^2}{l^2} - a\frac{l^2}{n^2} - ad_1 \right). \tag{15}$$

From (7) and (15), $d_{2,n}^{H}(d_1) = -d_{2,n}^{T}(d_1)$. Thus, we can get the properties of $d_2 = d_{2,n}^{H}(d_1)$ from proposition 1. Similar as $d_2 = d_{2,n}^{T}(d_1)$, when $a > 0$, we can define

$$d_{2,H}^{*}(d_1) = \begin{cases} d_{2,1}^{H}(d_1), & d_1 > d_{1g}^{(1)}, \\ d_{2,j}^{H}(d_1), & d_{1g}^{(j)} \le d_1 \le d_{1g}^{(j-1)},\ j = 2,3,\cdots. \end{cases} \tag{16}$$

for $d_2 = d_{2,n}^{H}(d_1)$.

Under the assumption that u_* is asymptotically stable for $\tau = 0$, we have $d_2 > d_{2,n}^{T}(d_1)$, *i.e.*,

$$\frac{d_2 u_*}{1 + d_1 \frac{n^2}{l^2}} \cdot \frac{n^2}{l^2} - a + d_1 \frac{n^2}{l^2} > 0.$$

We can conclude that for fixed $n \in \mathbb{N}$, when $d_2 > \max\left\{ d_{2,n}^{T}(d_1), d_{2,n}^{H}(d_1) \right\}$, Equation (14) has a unique positive root

$$\omega_n = \sqrt{\left(\frac{d_2 u_*}{1 + d_1 \frac{n^2}{l^2}} \cdot \frac{n^2}{l^2} - a + d_1 \frac{n^2}{l^2} \right)\left(\frac{d_2 u_*}{1 + d_1 \frac{n^2}{l^2}} \cdot \frac{n^2}{l^2} + a - d_1 \frac{n^2}{l^2} \right)}, \tag{17}$$

and Equation (12) has a pair of purely imaginary roots $\pm i\omega_n$ at $\tau = \tau_{n,j}\ (j = 0,1,2,\cdots)$, where

$$\tau_{n,j} = \begin{cases} \dfrac{1}{\omega_n}\left(\arccos \dfrac{l^2}{n^2} \cdot \dfrac{\left(1 + d_1 \frac{n^2}{l^2}\right)\left(a - d_1 \frac{n^2}{l^2}\right)}{d_2 u_*} + 2j\pi \right), d_2 > \max\left\{ d_{2,n}^{T}(d_1), d_{2,n}^{H}(d_1) \right\} \\ \text{and } d_2 > 0, \\ \dfrac{1}{\omega_n}\left(2\pi - \arccos \dfrac{l^2}{n^2} \cdot \dfrac{\left(1 + d_1 \frac{n^2}{l^2}\right)\left(a - d_1 \frac{n^2}{l^2}\right)}{d_2 u_*} + 2j\pi \right), d_2 > \max\left\{ d_{2,n}^{T}(d_1), d_{2,n}^{H}(d_1) \right\} \\ \text{and } d_2 < 0. \end{cases} \tag{18}$$

Lemma 2. For $d_1 > 0$ and $a + b < 0$, assume that ω_n and $\tau_{n,j}$ are defined by (17) and (18), respectively. Define regions as follows:

$$D_0^{+} = \left\{ (d_1, d_2) \,|\, d_1 > al^2, d_{2,1}^{T}(d_1) < d_2 < d_{2,1}^{H}(d_1) \right\},$$

$$D_0^{-} = \left\{ (d_1, d_2) \,|\, d_1 > 0, d_{2,T}^{*}(d_1) < d_2 < d_{2,H}^{*}(d_1) \right\},$$

$$D_n^+ = \{(d_1,d_2) \mid d_1 > 0, d_2 > d_{2,1}^T(d_1)\} \cap \{(d_1,d_2) \mid d_1 > 0, d_2 > d_{2,n}^H(d_1)\},$$

$$D_1^- = \{(d_1,d_2) \mid d_1 > 0, d_2 > d_{2,H}^*(d_1)\}.$$

1) If $a \geq 0$, when $(d_1,d_2) \in D_n^+ / D_{n+1}^+$ $(n = 1,2,\cdots)$, Equation (12) has a pair of purely imaginary roots $\pm i\omega_k$ at $\tau = \tau_{k,j}$, $k = 1,2,\cdots,n$. When $(d_1,d_2) \in D_0^+$, all roots of Equation (12) have negative real parts for any $\tau \geq 0$.

2) If $a < 0$, when $(d_1,d_2) \in D_0^-$, all roots of Equation (12) have negative real parts for any $\tau \geq 0$. When $(d_1,d_2) \in D_1^-$, for $d_1 \in \left(d_{1g}^{(n+1)}, d_{1g}^{(n)}\right)$, there exists some $m \in U_{d_2}$ such that Equation (12) has a pair of purely imaginary roots $\pm i\omega_m$ at $\tau = \tau_{m,j}$, where

$$U_{d_2} = \{m \in N \mid d_{2,m}^H < d_2\}.$$

Proof. (i) When $a \geq 0$, it follows from (7) and (15) that for fixed d_1, $d_{2,n}^H(d_1)$ is increasing with the increasing of n. Therefore, when $d_2 < d_{2,1}^H$, $d_2 < d_{2,n}^H$ for any $n > 1$. Notice that the curves $d_2 = d_{2,1}^T$ and $d_2 = d_{2,1}^H$ intersect at

$$d_1 = \hat{d}_1 = al^2, \tag{19}$$

and $d_{2,1}^H > d_{2,1}^T$ for $d_1 > al^2$. Therefore, when $(d_1,d_2) \in D_0^+$, all roots of Equation (12) have negative real parts for any $\tau \geq 0$. In addition, for $(d_1,d_2) \in D_n^+ / D_{n+1}^+$ $(n = 1,2,\cdots)$, Equation (12) has a pair of purely imaginary roots $\pm i\omega_k$ at $\tau = \tau_{k,j}$. This confirms the conclusion (i).

(ii) If $a < 0$, when $d_{2,T}^* < d_2 < d_{2,H}^*$, Equation (14) has no positive roots, that is, Equation (12) has no corresponding purely imaginary roots. When $d_2 > d_{2,H}^*$, there exists some m such that $d_{2,m}^H < d_2$, then Equation (12) has a pair of purely imaginary roots $\pm i\omega_m$ at $\tau = \tau_{m,j}$. Combined with Theorem 1 (ii), the conclusion (ii) follows immediately.

Lemma 3 For $d_1 > 0$ and $a + b < 0$, assume that ω_n and $\tau_{n,j}$ are defined by (17) and (18), respectively. For $a \geq 0$, when (d_1,d_2) is located on the lower boundary of the region D_n^+ / D_{n+1}^+, *i.e.*, $d_2 = d_{2,1}^T$, for $d_{1,n+1}^{TH} \leq d_1 < d_{1,n}^{TH}$ $(n = 2,3,\cdots)$, Equation (12) has one zero root $\lambda_1 = 0$ and a pair of purely imaginary roots $\pm i\omega_k$ at $\tau = \tau_{k,j}$, $k = 2,\cdots,n$, $j \in \mathbb{N}_0$, where $d_{1,n}^{TH} = \dfrac{l^2(a-1) + l^2\sqrt{a^2 + 1 + an^2 + \dfrac{a}{n^2}}}{n^2+1}$.

Proof. By (7) and (12), when $d_2 = d_{2,1}^T$, $\lambda_1 = 0$ is always the root of (12) for any $\tau \geq 0$. Notice that the curve $d_2 = d_{2,1}^T$ and $d_2 = d_{2,n}^H$ intersect at $d_1 \triangleq d_{1,n}^{TH}$, and the curve $d_2 = d_{2,1}^T$ is divided into several parts by the intersections $d_{1,n}^{TH}$. For the segement of $d_2 = d_{2,1}^T$ with $d_{1,n+1}^{TH} \leq d_1 < d_{1,n}^{TH}$, $d_2 = d_{2,1}^T$ is above the curves $d_2 = d_{2,k}^T(d_1)$, $k = 2,\cdots,n$, which means that $d_2 > d_{2,k}^T(d_1)$, $k = 2,\cdots,n$, and thus Equation (12) has a pair of purely imaginary roots $\pm iw_k$ at $\tau = \tau_{k,j}$,

$k=2,\cdots,n$, $j\in\mathbb{N}_0$.

Taking the derivative of both sides of Equation (12) with respect to τ, we get

$$\left[\frac{\mathrm{d}\lambda}{\mathrm{d}\tau}\right]^{-1}=\frac{1+d_1\frac{n^2}{l^2}-d_2u_*\frac{n^2}{l^2}\tau\mathrm{e}^{-\lambda\tau}}{d_2u_*\frac{n^2}{l^2}\lambda\mathrm{e}^{-\lambda\tau}}=\frac{1+d_1\frac{n^2}{l^2}}{d_2u_*\frac{n^2}{l^2}\lambda\mathrm{e}^{-\lambda\tau}}-\frac{\tau}{\lambda},$$

we have the following transversality condition

$$\frac{\mathrm{d}\,\mathrm{Re}\,\lambda}{\mathrm{d}\tau}\bigg|_{\tau=\tau_{n,j}}=\mathrm{Re}\left(\left[\frac{\mathrm{d}\lambda}{\mathrm{d}\tau}\right]^{-1}\bigg|_{\tau=\tau_{n,j}}\right)=\left(\frac{1+d_1\frac{n^2}{l^2}}{d_2u_*}\right)^2\cdot\frac{l^4}{n^4}>0.$$

Theorem 2. Assume that $a+b<0$.

i) For $a\geq 0$

a) When $(d_1,d_2)\in D_0^+$, u_* is asymptotically stable for $\tau\geq 0$;

b) When $d_2<d_{2,1}^T$, u_* is unstable for $\tau\geq 0$;

c) When $(d_1,d_2)\in D_n^+$, u_* is asymptotically stable for $\tau\in\left[0,\tau_n^*\right)$, and unstable for $\tau\in\left(\tau_n^*,\infty\right)$, and (2) undergoes Hopf bifurcation at $\tau=\tau_{k,j}$ with $k=1,\cdots,n$, $j\in\mathbb{N}_0$, where $\tau_n^*=\min\left\{\tau_{1,0},\cdots,\tau_{n,0}\right\}$;

d) On the lower boundary of the region D_n^+/D_{n+1}^+, *i.e.*, $d_2=d_{2,1}^T$, for fixed d_1, $d_{1,n+1}^{TH}\leq d_1<d_{1,n}^{TH}$ with $n=2,3,\cdots$, (2) undergoes Turing-Hopf bifurcation at $(\tau,d_2)=\left(\tau_{k,j},d_{2,1}^T(d_1)\right)$ with $k=2,\cdots,n$, $j\in\mathbb{N}_0$.

ii) For $a<0$:

a) When $(d_1,d_2)\in D_0^-$, u_* is asymptotically stable for $\tau\geq 0$;

b) When $d_2<d_{2,T}^*(d_1)$, u_* is unstable for $\tau\geq 0$;

c) When $(d_1,d_2)\in D_1^-$, for fixed $d_1\in\left(d_{1g}^{(n)},d_{1g}^{(n-1)}\right)$ with $n\in\mathbb{N}$, when $d_2>d_{2,n}^H(d_1)$, there exists a critical value τ_* of delay such that u_* is asymptotically stable for $0<\tau<\tau_*$ and unstable for $\tau>\tau_*$. Furthermore, (2) undergoes delay-induced Hopf bifurcation at $\tau=\tau_*$, where $\tau_*=\min\limits_{m\in U_{d_2}}\left\{\tau_{m,0}\right\}$;

d) On the lower boundary of D_0^-, *i.e.*, $d_2=d_{2,T}^*(d_1)$, system (2) undergoes Turing bifurcation at $d_2=d_{2,n}^T(d_1)$, and undergoes Turing-Turing bifurcation at the intersection of $d_2=d_{2,n}^T(d_1)$.

3. Example

3.1. Numerical Method

The coupled model (2) is reformulated into an equivalent parabolic-elliptic system and solved numerically. Introducing the auxiliary variable $v(x,t)=K\circ u(x,t)$, and applying the operator $-d_1\partial_{xx}+I$ to the convolution integral, the Green's function identity (3) yields the elliptic equation $d_1v_{xx}-v+u=0$. Consequently, the original delayed equation is recast as

$$\begin{cases} u_t = d_1 u_{xx} + d_2\left(u_x\left(v_\tau\right)_x + u\left(v_\tau\right)_{xx}\right) + f\left(u,\bar{u}\right), & x\in\left(0,l\pi\right), t>0, \\ 0 = d_1 v_{xx} - v + u, & x\in\left(0,l\pi\right), t>0, \\ u_x\left(0,t\right) = u_x\left(l\pi,t\right) = v_x\left(0,t\right) = v_x\left(l\pi,t\right) = 0, & t>0 \\ u\left(x,t\right) = \varphi\left(x\right), & x\in\left(0,l\pi\right), t\in\left[-\tau,0\right], \end{cases}$$

where $v_\tau = v\left(x,t-\tau\right)$ and $\bar{u} = G\circ u = \frac{1}{l\pi}\int_0^{l\pi} u\mathrm{d}y$. The elliptical relation also provides the identity

$$\left(v_\tau\right)_{xx} = \frac{v_\tau - u_\tau}{d_1}, \tag{20}$$

which avoids explicit second-order differentiation of v.

The interval $\left[0,l\pi\right]$ is divided uniformly into N grid points with spacing h. Second-order centered differences are adopted, and the Neumann boundary conditions are imposed by the method of ghost points (the derivatives at the endpoints remain zero). A semi-implicit scheme is employed with a fixed time step $\Delta t = 2\times 10^{-3}$. The diffusion term, the memory-based advection term, and the reaction-type tensor term and all linear in u are treated implicitly, whereas the nonlinear reaction term $f\left(u^n,\bar{u}^n\right)$ is treated explicitly:

$$\left(I - \Delta t\left[d_1 D_{xx} + d_2\mathrm{diag}\left(\left(v_\tau\right)_x\right)D_x + d_2\mathrm{diag}\left(\left(v_\tau\right)_{xx}\right)\right]\right)u^{n+1} = u^n + \Delta t f\left(u^n,\bar{u}^n\right).$$

The left-hand operator is tridiagonal, so each time step solves a tridiagonal linear system directly. Implicit treatment of the diffusion/advection operators removes the standard diffusive CFL restriction ($\Delta t < Ch^2$), allowing stable integration with the chosen step size. The elliptic equation $\left(-d_1 D_{xx} + I\right)v = u$ is solved at each step by a sparse LU decomposition (performed once, since the matrix is time-invariant), followed by back-substitution. Because Δt is fixed and τ is imposed as an integer multiple of Δt via the number of delay steps $nd = \mathrm{round}\left(\tau/\Delta t\right)$, the delayed field is retrieved from a ring buffer of length $nd+1$ storing the most recent u and v. The initial perturbation is $u_0\left(x\right) = 1 + 0.05\cos\left(\frac{nx}{l}\right)$. For $t\in\left[-\tau,0\right]$, the history is taken as $\varphi\left(x\right)\equiv u_0\left(x\right)$, and the elliptic initial condition is $v_0 = \left(-d_1 D_{xx} + I\right)^{-1} u_0$. Solutions are sampled every 0.5 time units for the spatiotemporal plots.

3.2. Numerical Results

In this section, we consider the single-species population model put forward by Britton in [10] [11]. The reaction function $f\left(u,G\circ u\right)$ of (2) is given by

$$f\left(u,G\circ u\right) = u\left[1 + cu - du^2 - \left(1+c-d\right)G\circ u\right]. \tag{21}$$

the term cu ($c>0$) represents a benefit to local aggregation, $-du^2$ ($d>0$) mitigates local aggregation, and $-\left(1+c-d\right)G\circ u$ under $0<d<1+c$ accounts for the disadvantage arising from nonlocal resource depletion. From (21), we have $u_* = 1$, and $a = c-2d$, $b = -1-c+d$.

Fix the parameters as $l=1, c=1.2$. Choosing $d=0.5$, then $a = 0.2 > 0$,

$b=-1.7$. Turing bifurcation curves are illustrated in Figure 1. From (19), $\hat{d}_1=0.2$.

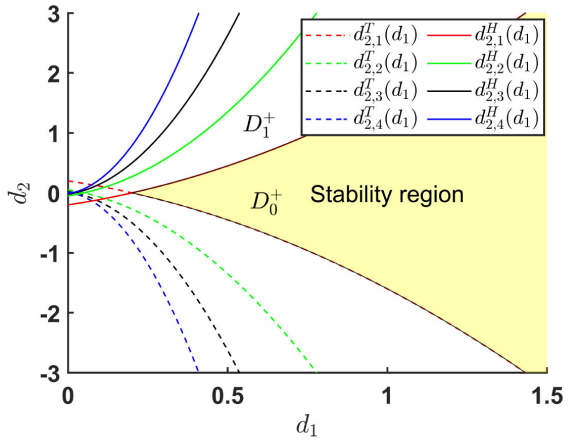


Figure 1. Stability regions and bifurcation curves for $a\geq 0$. The shadow region refers to the region where u_* is stable for all $\tau>0$.

1) $(d_1,d_2)=(1,0.4)\in D_0^+$ and $\tau=2.75$. u_* is asymptotically stable for $\tau\geq 0$ (see Figure 2(a));

2) $(d_1,d_2)=(1,-2)$, $d_{2,1}^T(d_1)=-1.6$ based on (7), $d_2=-2<d_{2,1}^T(d_1)=-1.6$. u_* is unstable and there exists spatially inhomogeneous steady state induced by Turing bifurcation (see Figure 2(b));

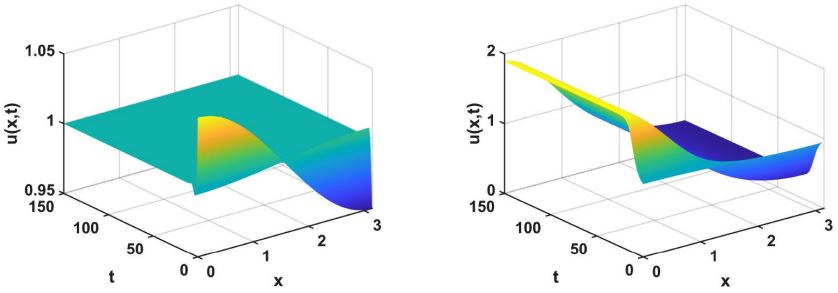


Figure 2. The rich dynamical phenomena when $a\geq 0$. (a) u_* is asymptotically stable for $(d_1,d_2)=(1,0.4)\in D_0^+$ and $\tau=2.75$. (b) Spatially inhomogeneous steady state for $(d_1,d_2)=(1,-2)$.

3) For fixed $d_1=0.1$, $d_{2,1}^T(d_1)=0.11$, we have

a) for $d_2\in(0,0.08]$, no Hopf bifurcation value can be found in this region;

b) for $d_2\in(0.08,0.11]$, there is a Hopf bifurcation value $\tau_{2,j}$ and $\tau_*=\tau_{2,0}$;

c) for $d_2\in(0.11,0.16]$, there are Hopf bifurcation values $\tau_{1,j},\tau_{2,j}$ and $\tau_*=\min\{\tau_{1,0},\tau_{2,0}\}$;

d) for $d_2 \in (0.16, 0.23]$, there are Hopf bifurcation values $\tau_{1,j}, \tau_{2,j}, \tau_{3,j}$ and $\tau_* = \min\{\tau_{1,0}, \tau_{2,0}, \tau_{3,0}\}$;

e) for $d_2 \in (0.23, 0.6]$, there are Hopf bifurcation values $\tau_{1,j}, \tau_{2,j}, \tau_{3,j}, \tau_{4,j}$ and

$$\tau_* = \min\{\tau_{1,0}, \tau_{2,0}, \tau_{3,0}, \tau_{4,0}\}.$$

Furthermore, it follows from Figure 3 that

$$\tau_* = \begin{cases} \tau_{2,0}, & d_2 \in (0.11, 0.21), \\ \tau_{3,0}, & d_2 \in (0.21, 0.4), \\ \tau_{4,0}, & d_2 \in (0.4, 0.6). \end{cases}$$

when we take $(d_2, \tau) = (0.13, 7.4) = P_1$, $(d_2, \tau) = (0.3, 2) = P_2$, and $(d_2, \tau) = (0.5, 1) = P_3$ respectively in Figure 3, system (2) has 2-mode, 3-mode and 4-mode spatially nonhomogeneous periodic solutions induced by Hopf bifurcation (see Figure 4).

4) System (2) undergoes Turing-Hopf bifurcation at $(d_2, \tau) = (0.11, 9.32)$, Hopf-Hopf bifurcation occurs when $(d_2, \tau) = (0.21, 3.33)$ and $(d_2, \tau) = (0.37, 1.24)$ (see Figure 3).

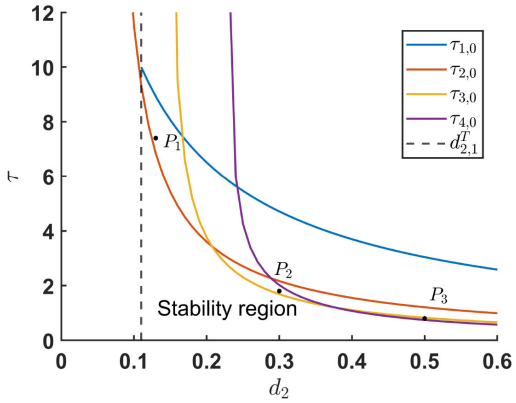


Figure 3. Stability regions and Hopf bifurcation curves for system (2). $d_1 = 0.1$.

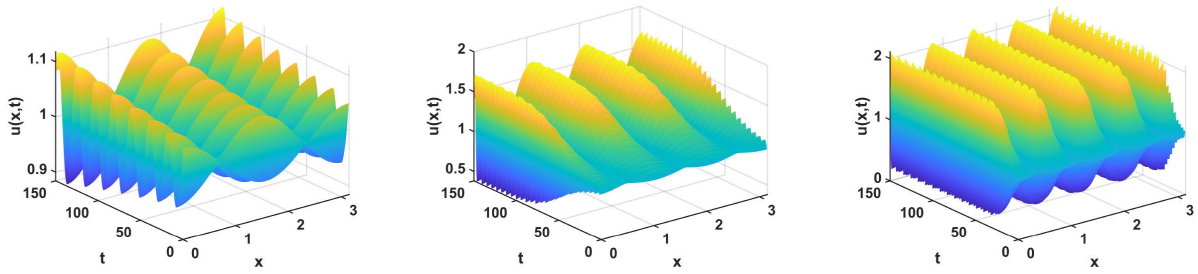


Figure 4. When $a \geq 0$, system (2) has (a) 2-mode spatially inhomogeneous periodic solution for $(d_2, \tau) = (0.13, 7.4) = P_1$; (b) 3-mode spatially inhomogeneous periodic solution for $(d_2, \tau) = (0.3, 2) = P_2$; (c) 4-mode spatially inhomogeneous periodic solution for $(d_2, \tau) = (0.5, 1) = P_3$.

Choosing $d=2$, thus $a=-2.8<0, b=-0.2$. Turing bifurcation curves are illustrated in Figure 5. From (9), we can get $d_{1g}^{(1)}=0.84$.

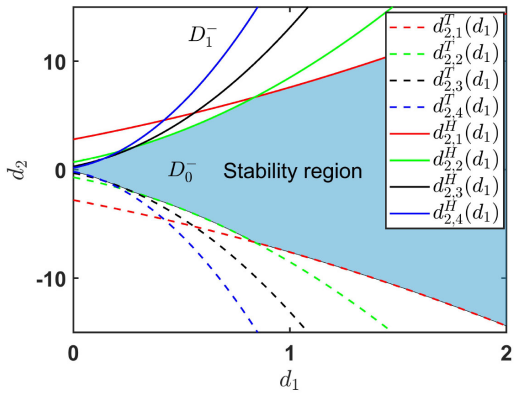


Figure 5. Stability regions and bifurcation curves for $a<0$. The shadow region refers to the region where u_* is stable for all $\tau>0$.

1) $(d_1,d_2)=(1,2)\in D_0^-$ and $\tau=1$, u_* is asymptotically stable for $\tau\geq 0$ (see Figure 6(a));

2) $(d_1,d_2)=(0.5,-4)$, $0.27=d_{1g}^{(3)}<d_1<d_{1g}^{(2)}=0.83$, $d_{2,T}^*(d_1)=d_{2,2}^T(d_1)=-3.6$ based on (11). u_* is unstable and there exists spatially inhomogeneous steady state induced by Turing bifurcation (see Figure 6(b));

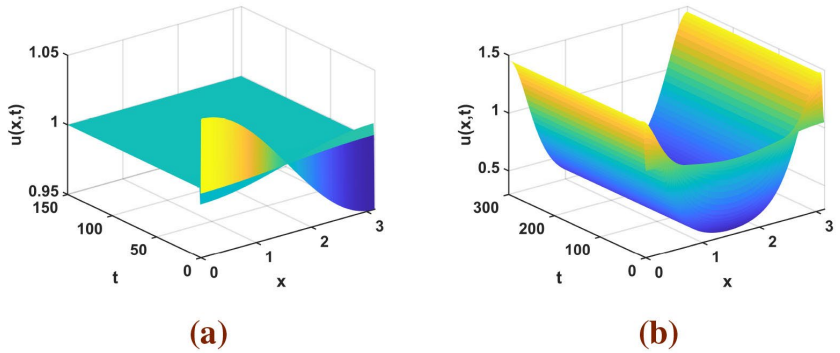


Figure 6. The rich dynamical phenomena when $a<0$. (a) u_* is asymptotically stable for $(d_1,d_2)=(1,2)\in D_0^-$ and $\tau=1$. (b) Spatially inhomogeneous 2-mode steady state for $(d_1,d_2)=(0.5,-4)$.

3) For fixed $d_1=0.66$, we have

a) for $d_2\in[0,4.98]$, there is no delay-induced Hopf bifurcation and the positive equilibrium $u_*=1$ is asymptotically stable for any $\tau\geq 0$;

b) for $d_2\in(4.98,5.82]$, there is a Hopf bifurcation value $\tau_{2,j}$ and $\tau_*=\tau_{2,0}$;

c) for $d_2\in(5.82,6.75]$, there are Hopf bifurcation values $\tau_{1,j},\tau_{2,j}$ and $\tau_*=\min\{\tau_{1,0},\tau_{2,0}\}$;

d) for $d_2 \in (6.75, 9.66]$, there are Hopf bifurcation values $\tau_{1,j}, \tau_{2,j}, \tau_{3,j}$ and

$$\tau_* = \min\{\tau_{1,0}, \tau_{2,0}, \tau_{3,0}\}.$$

e) for $d_2 \in (9.66, 40]$, there are Hopf bifurcation values $\tau_{1,j}, \tau_{2,j}, \tau_{3,j}, \tau_{4,j}$ and

$$\tau_* = \min\{\tau_{1,0}, \tau_{2,0}, \tau_{3,0}, \tau_{4,0}\}.$$

Furthermore, it follows from Figure 7 that

$$\tau_* = \begin{cases} \tau_{2,0}, & d_2 \in (4.98, 12.55), \\ \tau_{3,0}, & d_2 \in (12.55, 36.25), \\ \tau_{4,0}, & d_2 \in (36.25, 40). \end{cases}$$

when we take $(d_2, \tau) = (5.6, 2) = R_1$, $(d_2, \tau) = (14, 0.14) = R_2$, and $(d_2, \tau) = (37, 0.04) = R_3$ respectively in Figure 7, system (2) has 2-mode, 3-mode and 4-mode spatially nonhomogeneous periodic solutions induced by Hopf bifurcation (see Figure 8).

4) System (2) undergoes Hopf-Hopf bifurcation when $(d_2, \tau) = (12.51, 0.16)$ and $(d_2, \tau) = (36.22, 0.38)$ (see Figure 7).

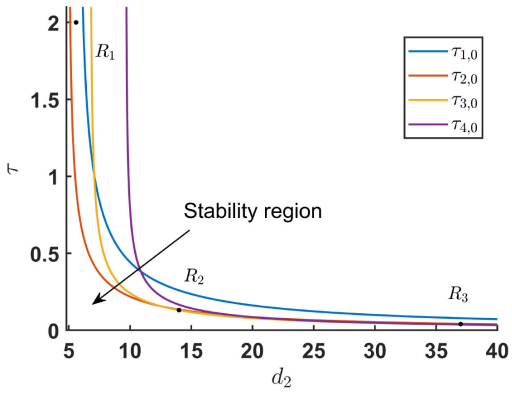


Figure 7. Stability regions and Hopf bifurcation curves for system (2). $d_1 = 0.66$.

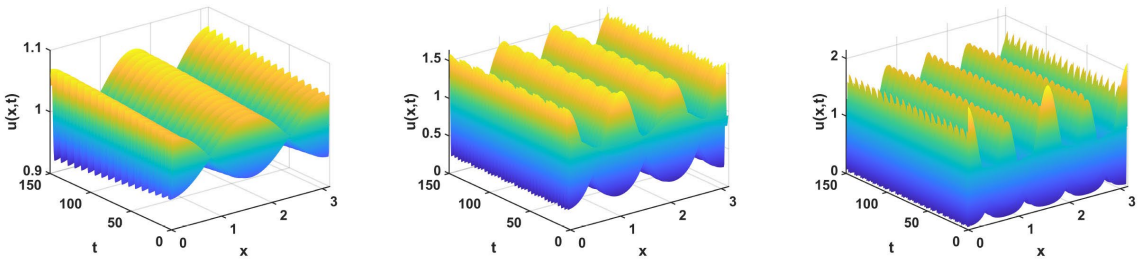


Figure 8. When $a < 0$, system (2) has (a) 2-mode spatially inhomogeneous periodic solution for $(d_2, \tau) = (5.6, 2) = R_1$; (b) 3-mode spatially inhomogeneous periodic solution for $(d_2, \tau) = (14, 0.14) = R_2$; (c) 4-mode spatially inhomogeneous periodic solution for $(d_2, \tau) = (37, 0.04) = R_3$.

4. Conclusions

In this paper, we mainly formulate a diffusive single-species model with nonlocal interactions and nonlocal spatial memory. We first explore spatial patterns for the system without delay. Comparative values of the random diffusion coefficient d_1, memory-driven diffusion coefficient d_2, and local interaction strength a jointly govern the stability of the spatially uniform steady state u_*. When $a \geq 0$, the boundary of the stability region is given by $d_{2,1}^T(d_1)$. For $a < 0$, the boundary of the stability region $d_{2,T}^*$ is formed by the intersections of $d_{2,n}^T(d_1)$.

After incorporating the memory delay effect, nonlocal interactions and nonlocal memory delay exert a combined influence on the stability of the homogeneous steady state u_*. Based on the symmetry of $d_{2,n}^T(d_1)$ and $d_{2,n}^H(d_1)$, we obtain the stability regions $D_0^+(a \geq 0)$ and $D_0^-(a < 0)$, at which u_* is locally asymptotically stable for any $\tau > 0$. We also get the incomplete stability regions D_n^+ and D_1^- on the d_1-d_2 parameter plane, at which there exists a critical value τ_*: the homogeneous steady state u_* is asymptotically stable if $0 \leq \tau < \tau_*$, and loses its stability with the emergence of Hopf bifurcation for $\tau > \tau_*$. When $(d_1, d_2) \in D_n^+$, delay-induced spatially inhomogeneous Hopf bifurcation and Turing-Hopf bifurcation take place. For $(d_1, d_2) \in D_1^-$, spatially inhomogeneous Hopf bifurcation arises, whereas Turing-Hopf bifurcation does not exist. In regions D_n^+ and D_1^-, Hopf bifurcations of various modes as well as Hopf-Hopf bifurcations can occur.

This work carries several simplifying assumptions that constrain its ecological interpretation. First, we consider only a one-dimensional habitat, while real animal populations move in 2-dimensional or 3-dimensional space. Second, the interaction kernel adopted here is spatially uniform, ignoring spatial heterogeneity of resources or terrain. Third, the memory delay τ is treated as a fixed constant, although memory retention may vary with location, time or population status in natural ecosystems. These idealizations limit the direct applicability of our model to animal movement within complex heterogeneous environments. Future extensions could relax these assumptions by introducing two-dimensional domains, state-dependent memory delay and spatially varying interaction kernels.

Funding

The work is supported by National Natural Science Foundation of China (Nos. 12571538 and 11901369).

Author Contributions

Jiajia Tang: Conceptualization, theoretical derivation, writing—original draft; Methodology, numerical simulation, writing—review and editing;

Yanfei Du: Formal analysis, validation, supervision, funding acquisition;

All authors read and approved the final manuscript.

Conflicts of Interest

The authors declare no conflicts of interest regarding the publication of this paper.

References

[1] Fagan, W.F., Lewis, M.A., Auger-Méthé, M., Avgar, T., Benhamou, S., Breed, G., *et al.* (2013) Spatial Memory and Animal Movement. *Ecology Letters*, **16**, 1316-1329. https://doi.org/10.1111/ele.12165

[2] Shi, J., Wang, C., Wang, H. and Yan, X. (2019) Diffusive Spatial Movement with Memory. *Journal of Dynamics and Differential Equations*, **32**, 979-1002. https://doi.org/10.1007/s10884-019-09757-y

[3] Song, Y., Wu, S. and Wang, H. (2019) Spatiotemporal Dynamics in the Single Population Model with Memory-Based Diffusion and Nonlocal Effect. *Journal of Differential Equations*, **267**, 6316-6351. https://doi.org/10.1016/j.jde.2019.06.025

[4] An, Q., Wang, C. and Wang, H. (2020) Analysis of a Spatial Memory Model with Nonlocal Maturation Delay and Hostile Boundary Condition. *Discrete and Continuous Dynamical Systems*, **40**, 5845-5868. https://doi.org/10.3934/dcds.2020249

[5] Shi, Q., Shi, J. and Wang, H. (2021) Spatial Movement with Distributed Memory. *Journal of Mathematical Biology*, **82**, Article No. 33. https://doi.org/10.1007/s00285-021-01588-0

[6] Shi, Q. and Song, Y. (2023) Spatial Movement with Nonlocal Memory. *Discrete and Continuous Dynamical Systems—B*, **28**, 5580-5596. https://doi.org/10.3934/dcdsb.2023067

[7] Xue, S., Song, Y. and Wang, H. (2024) Spatio-Temporal Dynamics in a Reaction-Diffusion Equation with Nonlocal Spatial Memory. *SIAM Journal on Applied Dynamical Systems*, **23**, 641-667. https://doi.org/10.1137/22m1543860

[8] Ni, W., Shi, J. and Wang, M. (2018) Global Stability and Pattern Formation in a Nonlocal Diffusive Lotka-Volterra Competition Model. *Journal of Differential Equations*, **264**, 6891-6932. https://doi.org/10.1016/j.jde.2018.02.002

[9] Chen, S. and Shi, J. (2013) Global Attractivity of Equilibrium in Gierer-Meinhardt System with Activator Production Saturation and Gene Expression Time Delays. *Nonlinear Analysis: Real World Applications*, **14**, 1871-1886. https://doi.org/10.1016/j.nonrwa.2012.12.004

[10] Britton, N.F. (1989) Aggregation and the Competitive Exclusion Principle. *Journal of Theoretical Biology*, **136**, 57-66. https://doi.org/10.1016/s0022-5193(89)80189-4

[11] Britton, N.F. (1990) Spatial Structures and Periodic Travelling Waves in an Integro-Differential Reaction-Diffusion Population Model. *SIAM Journal on Applied Mathematics*, **50**, 1663-1688. https://doi.org/10.1137/0150099